European Journal of Soil Science

WILEY

RESEARCH ARTICLE OPEN ACCESS

Root-Soil Contact as a Driver of Rhizosphere Structure and Plant Performance Traits in Contrasting Soil Structures

Maxime Phalempin[1] | Eva Lippold[1] | Doris Vetterlein[1,2] | Steffen Schlüter[1]

[1]Helmholtz Center for Environmental Research (UFZ), Halle (Saale), Sachsen-Anhalt, Germany | [2]Department of Soil Science, Martin-Luther-University Halle-Wittenberg, Halle (Saale), Sachsen-Anhalt, Germany

Correspondence: Maxime Phalempin (maxime.phalempin@ufz.de)

Received: 3 September 2025 | **Revised:** 17 December 2025 | **Accepted:** 18 December 2025

Keywords: maize | plant transpiration | root growth | root-soil interaction | shoot growth | soil compaction | soil structure | X-ray CT

ABSTRACT

Root-soil contact is a key factor in determining resource acquisition in soils; however its influence on the rhizosphere structure and the emerging plant traits are poorly understood. The present study aims to provide a comprehensive understanding of the coupled dynamics between plant roots and soil structure, with an emphasis on root-soil contact as a main explanatory variable. We investigated a fine-textured loam with a deformable soil matrix and a coarse-textured sand with rigid grains, with various degrees of compaction, structure heterogeneity, and fraction of fine particles. Over 21 days, we grew maize plants under well-watered conditions and monitored plant performance traits. After the growth period, we extracted undisturbed soil samples and scanned them with high resolution (10 μm) X-ray CT to characterize root-soil contact and root morphology. Our results show that in compressible soils, roots deform the surrounding soil matrix and induce rhizosphere compaction, whereas in non-compressible soils, the roots undergo deformation as they grow into zones with pores narrower than themselves. Increased root-soil contact did not result in increased plant transpiration or shoot biomass. Our study underscores the complex role of root-soil contact in shaping resource acquisition, and highlights the need to better understand the thresholds at which root-soil contact becomes limiting and how this depends on soil texture. It also emphasizes the influence of soil structure on root development and shows promising avenues for future work aimed at linking pore-scale heterogeneity and gas diffusion to root growth.

1 | Introduction

The root–soil contact is the proportion of the root surface that is in direct physical contact with the surrounding soil. Root-soil contact directly influences the plant's ability to access water and nutrients from the surrounding soil matrix through capillary flow (Carminati et al. 2010). Early investigations have shown that poor root-soil contact, such as in dry or loosely packed soils, can limit root water uptake and therefore plant performance (Schoonderbeek and Schoute 1994). Root-soil contact also affects other root functions such as root respiration, rhizodeposition, and the interaction with the soil biota. A great root-soil contact may restrict the diffusion of oxygen towards the root surface (Bartholomeus et al. 2008; Veen et al. 1992) and impose a greater resistance to root penetration into the soil (Stirzaker et al. 1996). Conversely, a lower root-soil contact reduces nitrogen-cycling by the prokaryotic community in the rhizosphere (Wendel et al. 2025) and the input of plant-derived carbon in the soil (Lucas et al. 2023). This highlights the complex role of root–soil contact as a facilitator of resource acquisition, a driver of rhizosphere microbial activity, and a potential mechanical barrier, all of which depend on the soil structure encountered by roots.

The quantification of root-soil contact is not an easy task because of the fragile and opaque nature of the soil. This makes it difficult to observe root systems and their immediate surroundings without disturbing their natural configuration. Early works on the characterization of root-soil contact have

Highlights

- Differences in root-soil contact did not affect plant transpiration under well-watered conditions.
- Soil structure modification had greater impacts on root traits than on shoot traits.
- Roots deform themselves if they cannot move or rearrange the rigid soil particles.

used soil thin-sections (Veen et al. 1992; Kooistra et al. 1992). Nowadays, X-ray computed tomography (CT) allows us to image the root-soil interface at high resolution in 3D without disturbing the soil structure (Lucas and Vetterlein 2022). From 3D X-ray CT images, Schmidt et al. (2012) characterized the root-soil contact for maize (*Zea mays* L.) and lupine (*Lupinus albus* L.) roots grown in substrates with different aggregate sizes. They found that differences in root-soil contact could not be explained solely by the decrease in porosity with decreasing aggregate size but could also have been the result of changes in the packing of particles around roots. In a synthetic review, Gregory et al. (2013) have aggregated the data of Schmidt et al. (2012) and found that root elongation rates increased with root-soil contact for maize and lupine plants, if the penetration resistance of the soil was low enough to not restrict root growth. They suggested that this was due to the fact that greater root-soil contact allowed faster uptake of both water and nutrients, which was beneficial for root growth. Koebernick et al. (2018) used X-ray CT to study the evolution of the root-soil contact of faba bean (*Vicia faba* L.) roots as a result of soil drying. They could show that root-soil contact decreased significantly over the course of the drying period. They could also show that root-soil contact was lower for tap roots than for lateral roots and they attributed this to the emergence of laterals that reorganized soil particles at the location of branching. Together, these studies highlight the potential of X-ray CT to reveal how root traits, soil structure, and environmental factors interact to shape root-soil contact.

As roots grow into the soil, they exert mechanical stress and rearrange soil particles, leading to localized changes in bulk density (Helliwell et al. 2017; Aravena et al. 2014). Recent studies with X-ray CT have shown that bulk density modifications induced by roots manifested themselves by a zone of low bulk density at the direct root-soil interface due to imperfect particle packing (Koebernick et al. 2019; Phalempin et al. 2021b; Lucas et al. 2019). The zone of low bulk density was then followed by an overshoot, which clearly indicated rhizosphere soil compaction. The overshoot was followed by a gradual decrease towards the density of the bulk soil. These studies have shown that the magnitude at which roots alter the soil microenvironment depends on the soil texture and structure. However, they left out a detailed analysis of the influence of root-soil contact on rhizosphere soil structure. From a geometrical perspective, it can be assumed that if a root encounters a few soil particles (resulting in low root-soil contact) along its growth trajectory, it can only induce a low degree of rhizosphere compaction. This is because the deformation needed to accommodate the loss of pore volume caused by the root can occur in the large pores directly in its vicinity. In contrast, if a root encounters a great number of soil particles (resulting in great root-soil contact) along its growth trajectory, it can induce a higher degree of rhizosphere compaction (see graphical abstract). This is because there is less pore space available and soil particles transfer the stress towards a larger volume to accommodate the deformation generated by the root. This suggests that there is a link between the root-soil contact and the rhizosphere densification; however, this link has remained poorly explored so far.

A detailed analysis of the literature cited above revealed that most studies on root-soil contact and rhizosphere structure properties have focused primarily on rather descriptive observations, with relatively little emphasis on the emerging plant traits. To our knowledge, no studies have attempted to link root-soil contact to both root and soil characteristics and the structural properties of the rhizosphere. Moreover, existing studies modulated simultaneously one or two experimental factors at most (one or two plant species in a given structure or texture). Currently, there is a lack of studies that present a more holistic analysis of the factors influencing root-soil physical interaction. Generating knowledge on which soil or root properties govern the feedback between root-soil contact and rhizosphere properties—and how this depends on soil texture and structure—is a prerequisite step for the explicit modeling of root growth in structured soils. Such mechanistic insights are essential to improve crop growth models with spatially explicit representations of the pore and root system architecture (Landl et al. 2017, 2021; Phalempin et al. 2023; de Willigen et al. 2018).

The present study aims to provide a comprehensive understanding of the coupled dynamics between plant roots and soil structure, with an emphasis on root-soil contact as a main explanatory variable. Specifically, we aimed to (1) develop a methodology to identify and quantify root–soil contact as a primary driver of rhizosphere densification. Furthermore, we aimed to (2) investigate how the interplay between pore and root geometries governs the emergence of root–soil contact and the spatial distribution of contact patches. Finally, we aimed to (3) characterize how changes in soil texture and structure influence plant development, as reflected in shoot and root trait responses. We hypothesized that soil structure exerts a major influence on plant and root growth, and that this influence can be explained by variations in root–soil contact. Furthermore, we hypothesized that the deformability of both the soil matrix and root tissues plays a role in modulating root-soil contact, with direct consequences for rhizosphere soil structure.

To reach these objectives, we grew maize plants in homogenized soils with contrasting structures and different compression behavior. To support plant growth, we chose a loam with a deformable matrix and a sand with rigid grains. For these two soil textures, the soil structure was modulated in the laboratory so as to establish gradients in porosity and pore size distribution, with consequences on oxygen and water availability. After the plant growth period, we extracted a total of 193 undisturbed soil cores from five different structure treatments (three with deformable loam aggregates and two containing predominantly rigid sand grains). We scanned these samples with high resolution (10 μm)

TABLE 1 | Description of the experimental treatments, detailing soil texture, bulk density, particle size range, water content at packing, and the number of soil columns.

Treatment	Soil	Bulk density ($g\,cm^{-3}$)	Particle size range (mm)	Water content at packing ($g\,100\,g^{-1}$)	Number of soil columns
L_LBD	Loam	1.26	< 1	5	5
L_HBD_f	Loam	1.4	< 1	5	12
L_HBD_c	Loam	1.4	0.2–1	5	6
S_hom	Sand	1.5	< 1	0.1	6
S_het	Sand	1.5	< 1	5	5

Note: The first letters of the abbreviations refer to the soil texture, for which "L" and "S" refer to the loam and sand, respectively. The following letters refer to the treatments resulting from the manipulation of soil structure. The abbreviations "LBD" and "HBD" refer to the low and high density treatments, respectively. The letters "f" (fine) and "c" (coarse) are used to describe the loam treatments with and without the fine fraction, respectively. The abbreviations "hom" and "het" refer to the homogeneous (i.e., columns filled with dry sand) or heterogeneous (i.e., columns filled with moist sand) packing of the sand columns.

X-ray CT to characterize the root-soil contact and rhizosphere structure. By combining multiscale analysis and novel image processing workflows, our study provides a comprehensive methodology to investigate how root-soil contact shapes rhizosphere structure and influences plant performance traits.

2 | Materials and Methods

2.1 | Soil Column Preparation

The treatments for the loam soil texture were created after air-drying and sieving soil material obtained from the upper 50 cm of a haplic Phaeozem soil profile. The treatments for the sandy texture were created by mixing 83.3% quartz sand (WF 33, Quarzwerke Weferlingen, Germany) and 16.7% of the sieved loam (Vetterlein et al. 2021). Before packing the columns, the soil was fertilized to ensure optimal plant growth. Nitrogen, phosphorus, potassium, and magnesium were added at a dose twice as high in sand as compared to that in loam to compensate for the low nutrient concentration of quartz sand. Calcium and micronutrients were also applied, but only to sand. For the concentration of fertilizer used, the reader is referred to Lippold et al. (2021).

To establish gradients in porosity and pore size distribution, we prepared soil columns with various degrees of soil compaction, soil fine particle content, and initial gravimetric water content during packing. For a compressible substrate such as loam, we modulated the soil structure by compacting the soil during column filling. We also modulated the texture by sieving out the fraction of fine soil particles (< 200 μm), effectively rendering a coarser texture, but with chemical and biological properties similar to those of the original loam (see Table SM1.1 for comparison between before and after sieving). For a non-compressible substrate such as sand, we modulated the structure by changing the gravimetric water content at packing. This modified the propensity of sand grains to agglomerate and generated a pore size distribution broader than that if they were packed in a dry state (Table 1).

The soil columns consisted of acrylic glass tubes (25 cm in height, 7 cm inner diameter). A nylon mesh (30 μm mesh size) was placed at the bottom of each column to retain the soil. The columns were filled with soil up to a height of 23 cm. With this setup, the volume available for plant growth was 885 cm^3. The columns were planted with *Zea mays* L. B73 seeds after sterilization in oxygen peroxyde for 3 min and immersion in saturated calcium sulfate for 4 h. After planting the seeds, the surface of the soil was covered with quartz gravel to reduce evaporation.

2.2 | Plant Growth

Plants were grown in a climate chamber set to 22°C during the day and 18°C at night with a 12 h light-period, 350 $\mu M\ m^{-2}\ s^{-1}$ photosynthetically active radiation and a constant relative humidity of 65%. Columns were carefully watered from the top and bottom to reach an average volumetric water content of 22% and 18% for loam and sand, respectively. Transpiration demand was compensated every 2 days through watering to avoid drought stress. Water loss between each watering event was recorded to quantify evapotranspiration. The duration of growth was 21 days and the harvest was carried out on day 22 after planting.

2.3 | Root, Shoot and Soil Sampling

On day 22, the shoots were cut and dried at 65°C for 72 h to determine the dry weight. After cutting the shoot, the soil was pushed out of the acrylic column using a custom-made subsampling device (UGT GmbH, Germany). The subsampling device allowed to push the soil out into aluminum rings maintained at a fixed position above the soil column. With this method, undisturbed soil cores (inner diameter and height of 1.6 cm) were extracted at a depth of 5, 10, and 15 cm. The soil cores were then prepared according to the methodology described by Lippold et al. (2023). After sample preparation, they were placed in a plastic container and kept at 4°C to prevent root shrinkage or decay. The storage duration before X-ray CT scanning did not exceed 5 days.

To destructively sample the roots, the remaining soil layers within the columns were placed on a sieve with a mesh of 0.63 μm, and washed carefully with deionized water. The roots remaining on the sieve were then collected and stored in a 50% alcohol solution (i.e., diluted Rotisol). Subsequently, the roots were scanned at 720 dpi with a 35 μm resolution using a flatbed scanner (EPSON Perfection V700). Root length density and root diameter were analyzed using WinRhizo 2019 software (Regent Instruments,

Canada). Root dry weight was determined in a similar fashion as in Vetterlein et al. (2022), and was used to derive the root:shoot ratio.

2.4 | X-Ray CT Scanning

X-ray CT scanning was conducted using an industrial μCT scanner (X-TEK XTH 225, Nikon Metrology) equipped with a PerkinElmer 1620 Flat Panel X-ray Detector (1.750 × 2.000 pixels). The acquired images were reconstructed into 3D tomograms with an isotropic side length of 10 μm and an image depth of 8-bit. This was done using a filtered back projection algorithm in the CT Pro 3D software (Nikon Metrology). Converting to 8-bit grayscale significantly reduced storage requirements without substantial loss of information. During this conversion, the grayscale range was normalized using a percentile stretching method, for which the darkest and brightest 0.2% of the voxels were set to 0 and 255, respectively, with linear scaling applied to the intermediate values.

2.5 | Image Pre-Processing

Region of interests (ROI) were carefully defined for each image after visual inspection. ROIs were drawn to exclude regions close to the core wall where soil structure disturbance had possibly occurred due to friction along the wall. Some of the first and last slices of the stacks were also cropped to exclude structure artifacts due to sampling.

To ensure that soil constituents exhibited a consistent gray value throughout the dataset, a series of preprocessing steps were applied to the images. These steps included histogram mode normalization and corrections for gray value radial and vertical drifts. Mode normalization of the histogram was used to reduce contrast differences between samples, which arose from the percentile stretching method used during conversion to 8-bit. Radial drift correction normalized gray values across radial distances from the core center to its periphery to correct for beam hardening artifacts. Vertical drift correction standardized gray values along vertical distances from the top to the bottom of the sample, compensating for artifacts caused by the conical X-ray beam of the scanner. All preprocessing steps were performed using the Fiji distribution of the ImageJ software (Schindelin et al. 2012) together with custom macros written in ImageJ scripting language.

2.6 | Image Segmentation

Image semantic segmentation was performed using a supervised machine learning procedure for voxel classification. The method relies on a random forest classification and is implemented in the Labkit plugin (Arzt et al. 2022). Individual classifiers were trained for each soil texture. For both loam and sand, we identified three classes of interest, namely the soil matrix (solid), air-filled pores, and living roots. Note that for sand, the "soil matrix" class comprises both the sand grains and the sieved loam mixed within the quartz sand.

To train the classifiers, four substacks (1472 × 1472 × 300 in dimensions x, y, z, respectively) were selected for each soil texture and considered representative of the dataset, that is, together

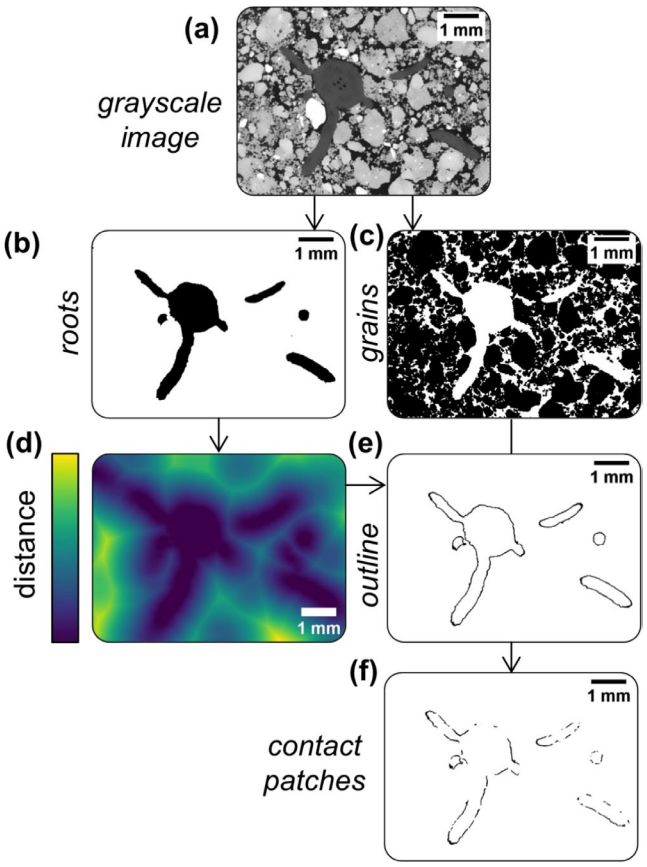

FIGURE 1 | Methodology for root-soil contact computation. Grayscale images (subfigure a) were segmented to isolate the roots (in black on subfigure b) and the soil matrix (in black on subfigure c). Root distance maps (subfigure d) were used to derive root outlines (in black on subfigure e) after thresholding with a threshold equal to 1. Root-soil contact patches (in black on subfigure f) were obtained by intersecting the root outlines (subfigure e) and the soil matrix (subfigure c) images.

they contained all the constituents of interest with different sizes and shapes. The substacks were then concatenated and annotated. Image annotation was performed using an interactive graphical user interface built within Labkit. Manual annotations on each material class were done until satisfactory segmentation results were achieved. The classifiers were designed to extract the original gray value intensity, Gaussian blurs, difference of Gaussians, gradient magnitude, Laplacian of Gaussian, Hessian eigenvalues, and variance at sigma levels of 1, 2, 4, 8, and 16. Each sigma level corresponds to a different spatial scale. The resulting classifiers were then applied to all other grayscale images (Figure 1a) of the dataset to distinguish the pore space, the roots (Figure 1b), and the soil matrix (Figure 1c).

2.7 | Image Post-Processing

For post-processing, object fragmentation was reduced by consecutive dilation, holes filling, and erosion steps in 3D. Due to the similar gray value range between roots and other types of particulate organic matter, the segmented root images contained false positives. Those were removed using a shape detection filter to distinguish cylindrical objects (roots) from blob-like or planar objects (e.g., seeds, leaf, or litter fragments). This filtering

step relied on two criteria: the "Vesselness" and the "Size" of the object. More information on this filter and its mathematical formulation is given elsewhere (Phalempin et al. 2021a). The values of the "Vesselness" and "Size" thresholds were adjusted so as to provide adequate results when compared to the original grayscale data.

2.8 | Quantitative Image Analysis

2.8.1 | Pore and Root Properties

Quantitative image analysis was carried out to derive pore and root properties. Mean pore (D_p) and root diameters (D_r) were quantified with the maximum inscribed sphere method (local thickness) implemented in the BoneJ plugin (Doube et al. 2010). Visible porosity (ϕ) was also calculated by dividing the volume of pores by the total volume of the ROI. The quantification of root length was carried out with a skeletonization step using the 'Analyze Skeleton' plugin of the BoneJ plugin suite.

2.8.2 | Root-Soil Contact

Root-soil contact was derived from X-ray CT images in a similar fashion as in Schmidt et al. (2012) (Figure 1). The outline of the segmented roots was determined after calculating the Euclidian Distance Transform (Figure 1d) using the "Exact Euclidean Distance Transform (3D)" function in ImageJ. The resulting distance maps were binarized with a threshold equal to 1 to obtain root outlines (Figure 1e). The root outlines were then intersected with the segmented soil matrix to obtain the root-soil contact patches (Figure 1f). The root-soil contact was calculated by counting the number of voxels of the contact patches. This value was then divided by the number of voxels that made up the root outlines and expressed as a percentage.

To quantify the physical interaction between root-soil contact and rhizosphere soil structure, we used two approaches. The first consisted in analyzing bulk density gradients around roots and quantifying the relationship between the root-soil contact and the root-induced compaction. The second approach consisted in analyzing the root morphology and the pore morphology around each root segment individually and relating these to root-soil contact. To simplify the language, we refer to these two approaches as the "sample" and "segment" approaches for the first and second approaches, respectively. For both approaches, the computation of root–soil contact followed the same method as described at Figure 1. The difference, however, was that for the sample approach, it was applied to all roots present within an undisturbed core, whereas in the segment approach, it was applied to individual root segments.

2.8.3 | The Sample Approach

For the sample approach, we measured bulk density gradients that extended from the root surfaces following an approach similar to that described by Lucas et al. (2019). Specifically, the analysis involved computing the Euclidean Distance Transform on binary images of the root system (Figure 1d). The resulting distance maps were then merged with the original grayscale image to create multichannel images. One channel contained grayscale intensity values and the other channel contained the corresponding distance to root values (noted x). A loop was performed in the X and Y directions across all Z-slices to calculate the average gray value as a function of the distance from the root surface. To make the results comparable between images with different contrast, gray values were normalized with the mean gray value of the entire image. Expressed in percentage, the result of this normalization represents the mean deviation from the gray value (noted dev) and can be used to assess root distance-dependent changes in soil density (Phalempin et al. 2023). Negative values for dev indicate zones of lower density, while positive values indicate zones of greater density, compared to the mean bulk density of the sample.

From the dev(x) function, we derived three metrics that we considered informative of the physical state of the rhizosphere. We defined dev_{peak} and x_{peak} as the maximum value of dev and the distance from the root surface at which this value was located, respectively. We also defined dev_{int}, which represents the area under the curve between two zero-crossing points x_1 and x_2. A graphical example for a typical root-induced compaction profile and the relevant metrics defined previously are shown in Figure 2. We consider dev_{int} to be indicative of the degree of soil compaction induced by roots, that is, a great value of dev_{int} indicates that a great volume of soil was displaced and compacted due to root penetration. However, a value close to zero indicates no root-induced soil compaction. The scheme for solving for dev_{int} is described in more details in the Supporting Information (Section SM1.2). Note that for this analysis, we only considered the samples that exhibited root-induced compaction. We considered samples with root-induced compaction as those for which x_{peak} was less than 0.5 mm. This choice was motivated by the data of Lucas et al. (2019) and Phalempin et al. (2021b), who showed that dev_{peak} is usually found within that distance for maize plants grown under conditions similar to the present study.

For the sample approach, we further characterized the root-soil contact with the workflow shown in Figure 1. We used this data to quantify the relationship between the root-soil

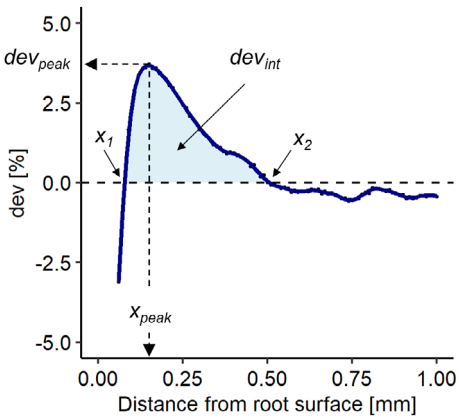

FIGURE 2 | Typical compaction profile induced by root growth in sieved and repacked soil. Data are from Phalempin et al. (2021b).

contact, dev_{peak}, x_{peak} and dev_{int}. At the sample scale, we also measured the mean pore diameter of the soil as well as the mean visible porosity using the methods described in the Section 2.8.1. This data was used to obtain information on how the different sieving and packing procedures impacted soil texture and structure.

2.8.4 | The Segment Approach

To perform the segment approach, we developed a new image processing workflow. This workflow allowed us to (1) isolate individual root segments in a 3D soil volume, (2) characterize their morphology (length and diameter), and (3) characterize the visible porosity and pore diameter of the soil around each root segment. By characterizing these properties around each root segment and not at the sample scale, we minimized the impact of local soil structure heterogeneity on the visible porosity and pore diameter measurements. With the segment approach, our objective was to characterize the properties of the soil outside the rhizosphere and use them as a proxy for the properties of the soil before root penetration induced structural disturbance. In the following, we use the term "rhizosphere" to refer to the zone of the soil around the roots that was physically impacted by root penetration. The workflow is described in details in the Supporting Information at the Section SM1.3. The segment approach was applied to a fifth of the dataset. The samples selected were the ones that contained a lot of roots so as to isolate many root segments at once. The data generated by this approach was used to quantify the relationship between the root-soil contact, the visible porosity (Vis. ϕ) and the pore diameter of the soil outside the rhizosphere (D_p), the root segment diameter (D_r) and the ratio of D_r / D_p. In addition, we selected root segments with the lowest and the greatest root-soil contact in order to visualize their associated contact patches with soil particles in 3D. This allowed to appreciate differences in root morphology as induced by root-soil contact.

2.9 | Data Analysis and Visualization

The analysis of the output data was carried out in R (R Core Team 2024). When applicable, differences in median between groups were evaluated using the non-parametric Mann–Whitney U (Mann and Whitney 1947) (for two groups) or Kruskal-Wallis tests (Kruskal and Wallis 1952) (for more than two groups). Post hoc pairwise multiple comparisons were performed after the methodology of Dunn (1964) and the resulting p-values were adjusted according to the procedure of Benjamini and Hochberg (2018). When relevant, the results are reported in the text with the notation "mean ± SE" to denote the mean of the distribution and the standard error around the mean. Three-dimensional renderings were performed with VGStudio Max (version 3.4, Volume Graphics GmbH, Heidelberg, Germany). To quantify the correlations between root-soil contact and the variables D_r, D_p, D_r / D_p, dev_{int}, dev_{peak} and x_{peak}, correlograms were build specific to each treatment but also pooling soil textures together. Correlations with p-value > 0.05 were excluded from the analysis and are therefore not displayed in the correlograms.

3 | Results

3.1 | Soil Structure

Soil structural differences between treatments were visible on grayscale images (Figure 3a) as well as on 2D segmented cross-sections (Figure 3b) of representative samples. For loam, increasing the bulk density from 1.26 to 1.40 g cm^{-3} caused the mean visible porosity to decrease from 0.163 ± 0.006 to 0.154 ± 0.003 (p-value > 0.05). The removal of the fine fraction of the loam increased the porosity to 0.227 ± 0.003, corresponding to an increase of 47% for the same bulk density packing as the fine loam ($p < 0.001$). For the sand packed under dry conditions, the visible porosity was 0.29 ± 0.003, whereas it reached 0.30 ± 0.004 for the sand packed under wet conditions ($p > 0.05$) (Figure 3c).

Soil structure modifications affected the mean pore diameter similarly to the visible porosity, but with two noticeable differences. Increasing the bulk density from 1.26 to 1.40 g cm^{-3} induced a decrease of the mean pore diameter by 12% (p-value < 0.01, Figure 3d). When packed dry, the mean pore diameter of the sand amounted to 78 ± 1 μm and the values were close the median (Figure 3d). When packed moist, the mean pore diameter of the sand increased to 117 ± 2 μm and the values were much more scattered around the median. These structural differences are also visible on Figure 3b. Packing the sand in moist conditions effectively increased the pore size and broadened the pore size distribution.

3.2 | Plant and Root Growth

At 19 days after sowing, the cumulated amount of water lost through evapotranspiration did not differ between treatments (Figure 4a). For loam, increasing the bulk density from 1.26 to 1.40 g cm^{-3} caused the mean root length density to decrease from 9.05 ± 0.48 to 7.93 ± 0.80 cm cm^{-3} (p-value > 0.05). The removal of the fine fraction of the loam further decreased the mean root length density to 7.52 ± 1.41 g cm cm^{-3} (p-value > 0.05, Figure 4b). Packing the sand homogeneously or heterogeneously had a tremendous effect on the mean root length density. When the sand was homogeneous, the mean root length density amounted to 5.12 ± 0.63 cm cm^{-3}. When the sand was heterogeneous, the root length density increased by 58% and reached 8.84 ± 0.81 cm cm^{-3} (p-value < 0.001).

Differences in soil structure had more subtle effects on the shoot dry weight (Figure 4c) than on root length density. Plants grown in the compacted loam with the fine fraction tended to be smaller, compared to the plants grown in the compacted loam without the fine fraction. For the compacted loam with the fine fraction, the mean shoot dry weight amounted to 1.51 ± 0.10 g, whereas it amounted to 1.73 ± 0.12 and 1.80 ± 0.03 g, for non-compacted loam and the compacted loam without the fine fraction, respectively (p-value > 0.05). For the homogeneous sand, the mean shoot dry weight reached 1.89 ± 0.26 g whereas it reached 2.20 ± 0.29 g for the heterogeneous sand (p-value > 0.05).

For loam, increasing the bulk density from 1.26 to 1.40 g cm^{-3} caused an increase in the mean root diameter from 244 ± 5 to 271 ±

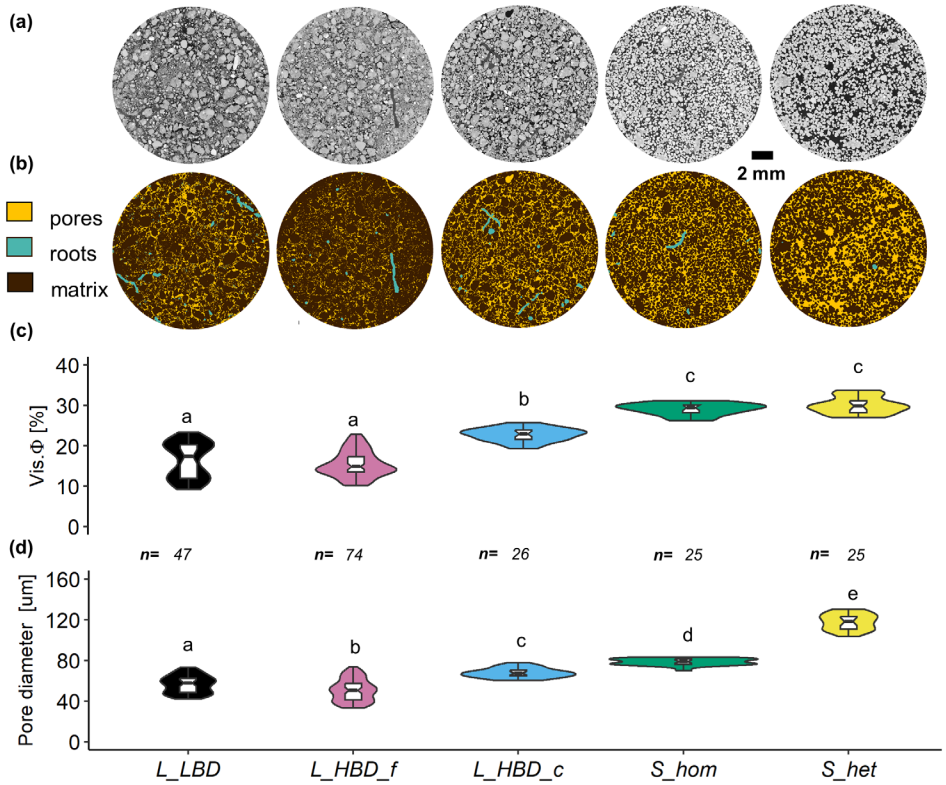

FIGURE 3 | Soil structure differences between treatments. Subfigure a shows 2D cross-sections of representative grayscale images for each treatment. Subfigure b shows 2D cross-sections of the segmented images shown in subfigure a. Note that the images of subfigure a and b are ordered in the same way as the labels of the x-axis of subfigure d. Subfigure c shows the distribution of visible porosity measured at the sample scale. The labels of the x-axis of subfigure d apply to subfigure c as well. Subfigure d shows the distribution of pore diameter measured at the sample scale for the treatments *L_LBD* ($n = 47$), *L_HBD_f* ($n = 74$), *L_HBD_c* ($n = 26$), *S_hom* ($n = 25$) and *S_het* ($n = 25$). The letters above the violins of subfigure c and d denote group membership according to the Pairwise Wilcoxon Rank Sum Tests with a threshold of 0.05.

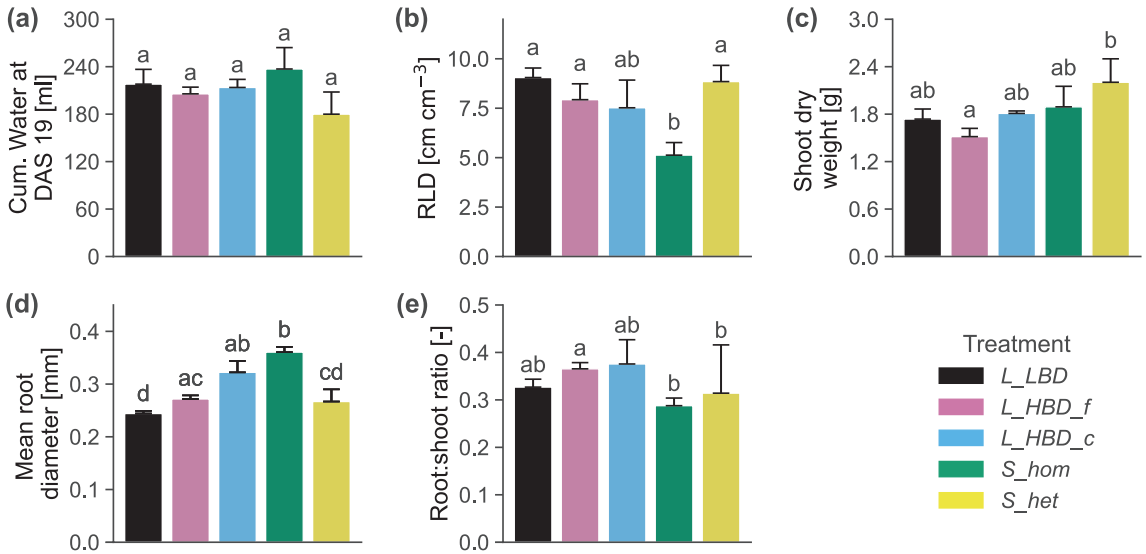

FIGURE 4 | Differences in the amount of water lost through evapotranspiration after 19 days after sowing (subfigure a), root length density (subfigure b), shoot dry weight (subfigure c), mean root diameter (subfigure d) and the root:shoot ratio (subfigure e) between treatments. The error bars denote the standard error around the mean of the measurements with $n = 6$ for *L_LBD*, $n = 12$ for *L_HBD_f*, $n = 5$ for *L_HBD_c*, $n = 6$ for *S_hom* and $n = 5$ for *S_het*. The letters above the bars denote group membership according to the Pairwise Wilcoxon Rank Sum Tests with a threshold of 0.05.

7 μm (p-value < 0.05). The removal of the fine fraction of the loam further caused an increase in mean root diameter to 322 ± 21 μm (Figure 4*d*). For the homogeneous sand, the mean root diameter reached 360 ± 10 μm. For the heterogeneous sand, the plants had finer roots than the plants grown in the homogeneous sand (p-value < 0.01) as the mean root diameter reached only 266 ± 23 μm only.

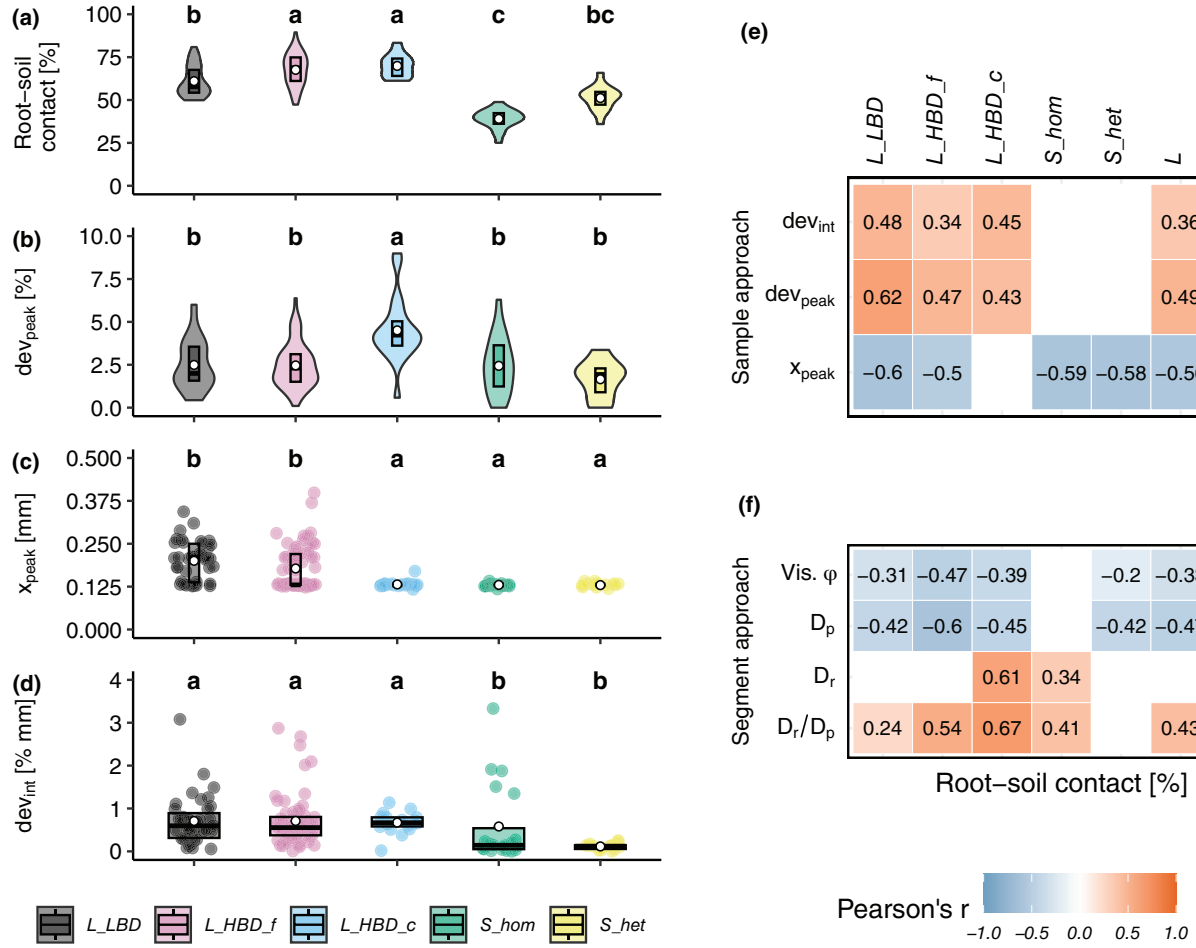

FIGURE 5 | Root-soil contact, rhizosphere soil compaction, root properties and their correlations. Subfigure a shows the root-soil contact, subfigure b shows the average peak deviation from the mean gray value (dev_{peak}), subfigure c shows the distance at which the peak of soil density was located (x_{peak}), and subfigure d shows the degree of soil compaction induced by roots (dev_{int}). These subfigures show data measured with the sample approach, with boxplots and a white dot to indicate the mean of the distribution. The letters above subfigure a–d denote group membership according to the Pairwise Wilcoxon Rank Sum Tests with a threshold of 0.05. For subfigures a–e, the number of samples analyzed for the treatments *L_LBD* (in black), *L_HBD_f* (in pink), *L_HBD_c* (in light blue), *S_hom* (in green) and *S_het* (in yellow) was 40, 64, 21, 21 and 16, respectively. For the subfigure *f*, the number of root segments analyzed for the treatments *L_LBD*, *L_HBD_f*, *L_HBD_c*, *S_hom* and *S_het* was 92, 219, 58, 40 and 128, respectively.

In loam, the differences in root:shoot ratio seemed more driven by differences in root thickness than by variations in shoot dry weight or root length (Figure 4e). The root:shoot ratio ranged from 0.30 to 0.42 and tended to increase as a result of soil compaction; however, the differences between loam treatments were not statistically significant. In sand, the differences in root length density were compensated by variations in root thickness. The resulting effect was that the root:shoot ratio did not differ between the sand treatments. The root:shoot ratio was slightly lower in sand than in loam, with values of 0.32 for the homogeneous sand and 0.25 for the heterogeneous sand.

3.3 | Root-Soil Contact and Rhizosphere Soil Compaction

For the non-compacted loam, the mean root-soil contact reached 61.1% ± 1.3% (Figure 5a). Increasing the bulk density from 1.26 to 1.40 g cm^{-3} caused an increase in the mean root-soil contact to 67.5% ± 1.1% (p-value < 0.001). Surprisingly, removing the fine fraction of the loam did not decrease the root-soil contact as the mean value reached 69.8% ± 1.4% and did not differ from the dense loam with the fine fraction (p-value > 0.05). The root-soil contact in sand was generally lower than in loam. For the homogeneous sand, the mean root-soil contact reached 39.3% ± 1.1%, whereas it was greater by 13% (p-value > 0.05) and reached 52.3% ± 1.7% for the heterogeneous sand (Figure 5a).

For the loam treatments containing the fine fraction, the average peak deviation from the mean gray value (dev_{peak}) reached 2.4% ± 0.2% (Figure 5b). Sieving out the fine fraction of the loam caused dev_{peak} to almost double, and reach 4.5% ± 0.4% (p-value < 0.001 for the comparisons with the loam treatments with the fine fraction). For the homogeneous sand, dev_{peak} reached 2.4% ± 0.3%, whereas it reached 1.6% ± 0.2% only, for the heterogeneous sand (Figure 5b). The distance from the root at which soil was the densest (x_{peak}) was clearly responding to whether the substrate used for plant growth contained fine particles or not. For the non-compacted loam, the mean

distance of the peak was 0.20 ± 0.008 mm. For the compacted loam with the fine fraction, this distance was reduced to 0.17 ± 0.007 mm (p-value > 0.05). For the compacted loam without the fine fraction, this distance was further reduced to 0.13 ± 0.001 mm and became closer to the values measured for sand. The x_{peak} values were not different between the compacted loam without the fine fraction and the sand treatments (p-value > 0.05). Interestingly, the degree of soil compaction induced by roots (dev_{int}) responded strongly to the soil texture (loam vs. sand), but seemed less affected by soil compaction or removal of the fine fraction. For the loam treatments, the mean values for dev_{int} were approximately equal to 0.70% ± 0.05% mm, and did not differ between treatments (p-value > 0.05). The mean value for dev_{int} in sand was equal to 0.32% ± 0.1% mm and the median was statistically lower than in loam (p-value < 0.05). The deviation from the mean gray value as a function of the distance from the root surface for all treatments are shown in the Supporting Information (Figure SM3).

3.4 | Correlations Between Root-Soil Contact, Root Diameter and Pore Morphology Outside the Rhizosphere

For the sample approach, correlation analysis between the root-soil contact and the rhizosphere structure variables dev_{int}, x_{peak} and dev_{peak} revealed patterns that were clearly specific to the soil compression behavior (Figure 5e). For the loam treatments, the root-soil contact was positively correlated to dev_{int}, with Pearson coefficients ranging from 0.34 from to 0.48. When the loam treatments were pooled together, the Pearson coefficient reached 0.36. Similarly, the root-soil contact was positively correlated to dev_{peak} in loam with Pearson coefficients ranging from 0.43 to 0.62, and reaching 0.49 when the loam treatments were pooled together. Interestingly, the root-soil contact was negatively correlated to x_{peak} with a Pearson coefficient reaching −0.56 for the loam treatments pooled. In sand, the root-soil contact was not correlated to dev_{int} and dev_{peak} (p-value > 0.05). This was true at the treatment level as well as when both sand treatments were pooled together (Figure 5e).

For the segment approach, correlation analysis between the root-soil contact, the root diameter, and the pore morphology outside the rhizosphere revealed common patterns for the root segments grown in loam, but less so in sand. For the loam treatments, the correlation between the root-soil contact and the visible porosity outside the rhizosphere had values ranging from −0.31 to −0.47 (Figure 5f). Pooling the loam treatments yielded a Pearson coefficient of −0.33. A somewhat stronger negative correlation was found for the relationship between the root-soil contact and the mean pore diameter of the soil outside the rhizosphere ($r = -0.47$). Another similarity for the loam treatments was found for the correlation between the root-soil contact and the ratio D_r / D_p. The Pearson coefficients were all positive for the loam treatments and reached 0.43 when they were pooled together. Pooling both sand treatments together, the correlations between the root-soil contact and *Vis.* ϕ, D_r and D_r / D_p were significant, yet quite low, with Pearson coefficients ranging from −0.17 to −0.22.

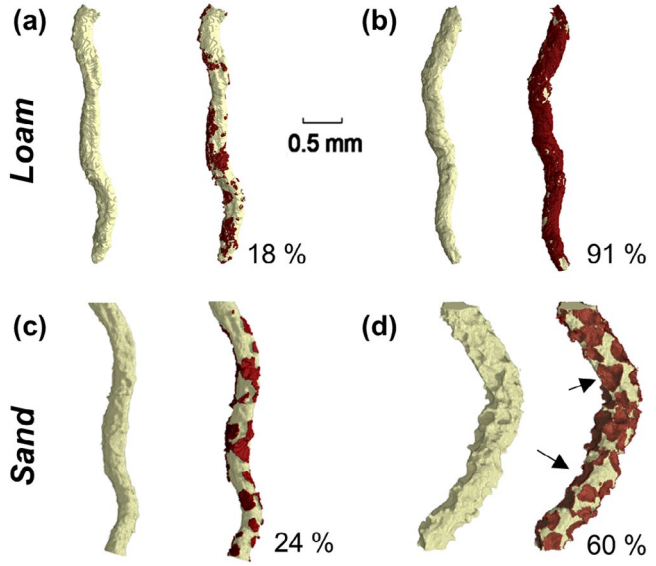

FIGURE 6 | Root morphology response to root-soil contact in soils with different compressibility. For all subfigures, the root segments on the left show the root volumes (in green) without the contact patches whereas the root segments on the right show the root volumes and the contact patches between the root surface and soil particles (in red). Subfigure a and b show root segments in loam having a root-soil contact of 18% and 91%, respectively. In the compressible loam, differences in root-soil contact did not result in visible changes in root morphology. Subfigure c and d show root segments in sand having a root-soil contact of 24% and 60%, respectively. In sand, great root-soil contact resulted in remarkable indentations in the root surface caused by the rigid sand grains (see black arrows on subfigure d).

3.5 | Root Morphology Response to Root-Soil Contact

Visual inspection of selected root segments provided insight into the impact of root-soil contact on root morphology, and how this was affected by soil structure and the compressibility of the substrate. In loam, differences in root morphology between root segments that had a low (18%, see Figure 6a) or a great (91%, see Figure 6b) root-soil contact were not noticeable visually. In sand, clear differences in root morphology between roots with low or great root-soil contact were observed. For a root with a low root-soil contact (24%, see Figure 6c), the root morphology did not seem impacted. However, for a root with a great root-soil contact (60%, see Figure 6d), the root surface exhibited some remarkable indentations. Parallel assessment with the original gray value image confirmed that these indentations were caused by the rigid sand grains.

4 | Discussion

In this study, we developed a method to analyze root-induced compaction and its relation to root–soil contact. This method allowed us to identify and quantify the root–soil contact as a driver of rhizosphere densification, and how it depended on soil structure and texture. For the compressible loam, we found a positive relationship between the root–soil contact and the peak of soil density in the vicinity of roots. This result is supported by

the previous (but less quantitative) work of Lucas et al. (2019) and Phalempin et al. (2021b). In a modeling study, Aravena et al. (2011) demonstrated that root-induced rhizosphere compaction enhanced water flow towards roots in loose soils. Given the positive correlation we observed between root–soil contact and rhizosphere densification, our result supports the idea that increased root–soil contact facilitates root water uptake (de Willigen et al. 2018; Carminati et al. 2010) not only by the increased availability of surface contact, but also by an active modification of rhizosphere hydraulic properties (Aravena et al. 2011; Landl et al. 2021). For sand, we found no relationship between the root–soil contact and the degree of rhizosphere compaction. This can be attributed to the fact that the roots merely caused slight tilting and rotation of the rigid sand grains, but were not able to displace them. The positive, yet relatively weak, correlation between root–soil contact and pore diameter outside the rhizosphere in sand may likewise result from this tilting (Figure 5f). The reorientation of sand grains at the root surface induces bigger pores past that zone of aligned grains. This finding was already described in one of our previous studies using the same substrates (see Figure 6*b* in Phalempin et al. (2021b)). Interestingly, removing the fine fraction from the loam made the radial compaction resemble the one observed in sand, while still preserving the high root–soil contact characteristic of the deformable loam.

By visualizing root segments and their associated contact patches in 3D, we showed that root–soil contact is influenced by the deformability of both the soil matrix and the root tissues. In loam, the higher degree of root–soil contact can be explained by its smaller aggregate sizes (Schmidt et al. 2012), which allowed aggregates to adjust and conform more closely to the root surface upon deformation (Figure 6b). Interestingly, we also observed that when roots grew in dense zones of rigid sand grains, they had the ability to deform in order to penetrate pores narrower than themselves. In some cases, this resulted in the presence of notable indentations in the root tissues, which increased root–soil contact, as the sand grains fit better to the surface of the deformed root (Figure 6d). Despite the fact that the effect of mechanical stress on root morphology has been studied and reviewed intensively (Potocka and Szymanowska-Pułka 2018), we are unaware of any study investigating this feature. Microscopy and transcriptomic approaches of targeted root segments could help reveal how localized mechanical stress alters root anatomical structure and gene expression at the cellular level (Zhu et al. 2025). Due to the potential consequences for nutrient uptake and water transport, this aspect deserves more attention for future research.

Our study not only provides insights into the feedback between root-soil contact and rhizosphere structure, but also provides opportunities to analyze plant trait responses to changes in soil physical conditions. In our experiment, changes in soil structure had greater impacts on roots than on shoots. In the fine-textured loam, we observed an increase in root diameter (Figure 4d) and a decrease in root length (Figure 4b) with increasing soil bulk density. This observation is in good agreement with other studies that found the same effect for a variety of monocots and dicots plants (Bengough et al. 2011; Materechera et al. 1991; Giuliani et al. 2024). This combination of effects manifested itself in an increase in root:shoot ratio, which was also documented by Rivera et al. (2019). In sand, soil structure differences drastically impacted root growth, but less so shoot biomass. When plants were grown in homogeneous sand, they tended to develop fewer but thicker roots compared to those grown in heterogeneous sand. This pattern is likely related to differences in aeration and gas exchange with the atmosphere. Possibly, oxygen diffusion and the escape of ethylene from the rhizosphere (Pandey et al. 2021) were restricted in the homogeneous sand. This could have led to a reduction of meristematic activity and elongation, while stimulating radial expansion (Jackson et al. 1981; Moss et al. 1988) and anatomical adjustments such as enlarged cortical cells (Zhang et al. 2025). In heterogeneous sand, the exchange of gases from the root apices to the atmosphere was likely promoted by the presence of much larger pores (Figure 3) with greater continuity. This particular pore space arrangement could have been responsible for increased root growth and the development of finer roots. These insights emphasize the influence of soil structure on root development and highlight promising avenues for future work aimed at linking pore-scale heterogeneity and gas diffusion processes to root growth.

Interestingly, differences in root-soil contact did not affect plant transpiration, shoot or root biomass. This partly contradicts the results of Gregory et al. (2013) and falsifies our first hypothesis. We suggest that this is due to the fact that we carried out the plant growth experiments in well-watered conditions and with additional mineral fertilization. Under these circumstances, root-soil contact might not have been limiting for water and nutrient uptake. Under more limiting conditions, it could be expected that differences in root-soil contact between loam and sand would exert more effects on plant performance traits. In coarse-textured soils such as sand, the unsaturated hydraulic conductivity drops more drastically at less negative water potential (Wankmuller et al. 2024; Carminati and Javaux 2020), which causes a decrease in rhizosphere conductance and root water uptake (Koch et al. 2025). Under these conditions, the lower root-soil contact in sand could become limiting and reveal differences with the fine-textured loam. This highlights the necessity to characterize root-soil contact thresholds at which water and nutrient uptake becomes restricted. It also highlights the need to characterize how these thresholds depend on the soil hydraulic properties and the shrinkage behavior of the roots (Carminati et al. 2013; Harrison Day et al. 2025) and their hairs (Duddek et al. 2023, 2022).

Our new methodology at the scale of individual root segments allowed us to demonstrate that the emergence of root-soil contact is governed by the interaction between pore and root geometries. We showed that root-soil contact is increased as big roots penetrate narrow pores (Figure 5f). Despite the little knowledge gain offered by this approach applied in sieved soils, we see a potential in applying this methodology (see Supporting Information SM1.3) to the study of roots grown in naturally structured soils. We envision that coupling this approach with spatial data on microscale soil strength (Phalempin et al. 2023) will help provide insights into root growth patterns in highly heterogeneous soils. Note also that our results obtained in the laboratory with sieved soils are likely overestimated in comparison to what happens in the field. In sieved soils, plant roots must

substantially reorganize the existing structure and create new macroporosity, whereas in intact soils these structural modifications have already been shaped by preceding vegetation or management (Geers-Lucas et al. 2025; Phalempin et al. 2025). This highlights the importance of extending such analyses to more natural settings, where legacy structure and biological history may strongly modulate the root-soil contact and root-induced pore modifications.

5 | Conclusion

Through a combination of high-resolution X-ray CT imaging and novel image processing workflows, we demonstrated that root-soil contact is shaped not only by soil texture and structure but also by the interaction between root and pore morphology. We have shown that, in deformable soils, roots encountering fewer soil particles (resulting in low root-soil contact) along their growth trajectory only induce a minor rhizosphere compaction, characterized by a small overshoot of soil density located further away from the root surface. In contrast, when roots encounter a greater number of particles (resulting in greater root-soil contact), rhizosphere compaction is more pronounced and occurs closer to the root surface. In granular soils, young maize roots have the ability to deform to penetrate zones of narrow pores if they are unable to move away and rearrange the rigid grains.

By integrating microscale measurements of root–soil contact with plant and root trait data, we have shown that root–soil contact was not decisive for resource acquisition under non-limiting conditions. Greater root–soil contact was not associated with greater shoot or root growth. We have also found evidence that the influence of soil structure on root growth is associated with changes in pore-scale heterogeneity, which subsequently alters gas diffusion and feeds back on root development.

Methodologically, our approaches at the root segment and root system scale combined with destructive sampling offer a robust and transferable framework for quantifying root–soil physical interactions. Future work should apply this framework to a wider range of soil types, plant species, environmental conditions and intact soil structure to better understand the role of root–soil contact in shaping resource acquisition and plant performance in field-relevant scenarios.

Author Contributions

Maxime Phalempin: conceptualization, investigation, writing – original draft, methodology, validation, visualization, writing – review and editing, software, formal analysis, data curation. **Eva Lippold:** writing – review and editing, methodology. **Doris Vetterlein:** supervision, resources, writing – review and editing, funding acquisition. **Steffen Schlüter:** funding acquisition, writing – review and editing, validation, supervision, resources, conceptualization.

Acknowledgments

The authors would like to thank Bernd Apelt and Yvonne Eckstein for their help with the characterization of the soil chemical analysis. Open Access funding enabled and organized by Projekt DEAL.

Funding

This project was carried out within the framework of the priority program 2089 "Rhizosphere Spatiotemporal Organization - A Key to Rhizosphere Functions" funded by DFG, German Research Foundation (Project no. 403801423).

Conflicts of Interest

The authors declare no conflicts of interest.

Data Availability Statement

The datasets used in this study are available from the authors upon reasonable request.

References

Aravena, J. E., M. Berli, T. A. Ghezzehei, and S. W. Tyler. 2011. "Effects of Root-Induced Compaction on Rhizosphere Hydraulic Properties - X-Ray Microtomography Imaging and Numerical Simulations." *Environmental Science & Technology* 45, no. 2: 425–431.

Aravena, J. E., M. Berli, S. Ruiz, F. Suárez, T. A. Ghezzehei, and S. W. Tyler. 2014. "Quantifying Coupled Deformation and Water Flow in the Rhizosphere Using X-Ray Microtomography and Numerical Simulations." *Plant and Soil* 376, no. 1–2: 95–110.

Arzt, M., J. Deschamps, C. Schmied, et al. 2022. "LABKIT: Labeling and Segmentation Toolkit for Big Image Data." *Frontiers of Computer Science* 4: 777728.

Bartholomeus, R. P., J.-P. M. Witte, P. M. van Bodegom, J. C. Dam, and R. Aerts. 2008. "Critical Soil Conditions for Oxygen Stress to Plant Roots: Substituting the Feddes-Function by a Process-Based Model." *Journal of Hydrology* 360, no. 1: 147–165.

Bengough, A. G., B. McKenzie, P. Hallett, and T. Valentine. 2011. "Root Elongation, Water Stress, and Mechanical Impedance: A Review of Limiting Stresses and Beneficial Root Tip Traits." *Journal of Experimental Botany* 62, no. 1: 59–68.

Benjamini, Y., and Y. Hochberg. 2018. "Controlling the False Discovery Rate: A Practical and Powerful Approach to Multiple Testing." *Journal of the Royal Statistical Society. Series B, Statistical Methodology* 57, no. 1: 289–300.

Carminati, A., and M. Javaux. 2020. "Soil Rather Than Xylem Vulnerability Controls Stomatal Response to Drought." *Trends in Plant Science* 25, no. 9: 868–880.

Carminati, A., A. B. Moradi, D. Vetterlein, et al. 2010. "Dynamics of Soil Water Content in the Rhizosphere." *Plant and Soil* 332, no. 1: 163–176.

Carminati, A., D. Vetterlein, N. Koebernick, S. Blaser, U. Weller, and H.-J. Vogel. 2013. "Do Roots Mind the Gap?" *Plant and Soil* 367, no. 1: 651–661.

de Willigen, P., M. Heinen, and M. van Noordwijk. 2018. "Roots Partially in Contact With Soil: Analytical Solutions and Approximation in Models of Nutrient and Water Uptake." *Vadose Zone Journal* 17, no. 1: 1–16.

Doube, M., M. M. Kłosowski, I. Arganda-Carreras, et al. 2010. "BoneJ: Free and Extensible Bone Image Analysis in ImageJ." *Bone* 47, no. 6: 1076–1079.

Duddek, P., M. A. Ahmed, M. Javaux, et al. 2023. "The Effect of Root Hairs on Root Water Uptake Is Determined by Root–Soil Contact and Root Hair Shrinkage." *New Phytologist* 240, no. 6: 2484–2497.

Duddek, P., A. Carminati, N. Koebernick, et al. 2022. "The Impact of Drought-Induced Root and Root Hair Shrinkage on Root–Soil Contact." *Plant Physiology* 189, no. 3: 1232–1236.

Dunn, O. J. 1964. "Multiple Comparisons Using Rank Sums." *Technometrics* 6, no. 3: 241–252.

Geers-Lucas, M., A. Guber, and A. Kravchenko. 2025. "Root-Pore Interactions, the Underestimated Driver for Rhizosphere Structure and Rhizosheath Development." *Plant, Cell & Environment* 49: 295–308.

Giuliani, L. M., P. D. Hallett, and K. W. Loades. 2024. "Effects of Soil Structure Complexity to Root Growth of Plants With Contrasting Root Architecture." *Soil and Tillage Research* 238: 106023.

Gregory, P. J., C. J. Atkinson, A. G. Bengough, et al. 2013. "Contributions of Roots and Rootstocks to Sustainable, Intensified Crop Production." *Journal of Experimental Botany* 64, no. 5: 1209–1222.

Harrison Day, B. L., T. J. Brodribb, N. C. Walker, and C. R. Brodersen. 2025. "Fine Root Shrinkage Across Intact Root Networks Begins Early During Dehydration in Diverse Plants From Conifers to Angiosperms." *Plant, Cell & Environment*: 70254.

Helliwell, J., C. J. Sturrock, S. Mairhofer, et al. 2017. "The Emergent Rhizosphere: Imaging the Development of the Porous Architecture at the Root-Soil Interface." *Scientific Reports* 7: 14875.

Jackson, M. B., M. Drew, and S. C. Giffard. 1981. "Effects of Applying Etnylene to the Root System of *Zea mays* on Growth and Nutrient Concentration in Relation to Flooding Tolerance." *Physiologia Plantarum* 52, no. 1: 23–28.

Koch, A., G. Cai, M. A. Ahmed, et al. 2025. "On the Importance of Rhizosphere Conductance and Soil–Root Contact in Drying Soils." *Annals of Botany* 136: 1047–1064.

Koebernick, N., K. R. Daly, S. D. Keyes, et al. 2019. "Imaging Microstructure of the Barley Rhizosphere: Particle Packing and Root Hair Influences." *New Phytologist* 221, no. 4: 1878–1889.

Koebernick, N., S. Schlüter, S. R. G. A. Blaser, and D. Vetterlein. 2018. "Root-Soil Contact Dynamics of Vicia Faba in Sand." *Plant and Soil* 431, no. 1: 417–431.

Kooistra, M. J., D. Schoonderbeek, F. R. Boone, B. W. Veen, and M. Van Noordwijk. 1992. "Root-Soil Contact of Maize, as Measured by a Thin-Section Technique. Part 2: Effect of Soil Compaction." *Plant and Soil* 139, no. 1: 119–129.

Kruskal, W. H., and W. A. Wallis. 1952. "Use of Ranks in One-Criterion Variance Analysis." *Journal of the American Statistical Association* 47, no. 260: 583–621.

Landl, M., K. Huber, A. Schnepf, et al. 2017. "A New Model for Root Growth in Soil With Macropores." *Plant and Soil* 415, no. 1: 99–116.

Landl, M., M. Phalempin, S. Schlüter, et al. 2021. "Modeling the Impact of Rhizosphere Bulk Density and Mucilage Gradients on Root Water Uptake." *Frontiers in Agronomy* 3: 622367.

Lippold, E., M. Phalempin, S. Schlüter, and D. Vetterlein. 2021. "Does the Lack of Root Hairs Alter Root System Architecture of *Zea mays*?" *Plant and Soil* 467, no. 1: 267–286.

Lippold, E., S. Schlüter, C. W. Mueller, et al. 2023. "Correlative Imaging of the Rhizosphere - A Multimethod Workflow for Targeted Mapping of Chemical Gradients." *Environmental Science & Technology* 57, no. 3: 1538–1549.

Lucas, M., J. P. Santiago, J. Chen, A. Guber, and A. Kravchenko. 2023. "The Soil Pore Structure Encountered by Roots Affects Plant-Derived Carbon Inputs and Fate." *New Phytologist* 240, no. 2: 515–528.

Lucas, M., S. Schlüter, H.-J. Vogel, and D. Vetterlein. 2019. "Roots Compact the Surrounding Soil Depending on the Structures They Encounter." *Scientific Reports* 9, no. 1: 1–13.

Lucas, M., and D. Vetterlein. 2022. "X-Ray Imaging of Root-Soil Interactions." In *X-Ray Imaging of the Soil Porous Architecture*, 129–157. Springer.

Mann, H. B., and D. R. Whitney. 1947. "On a Test of Whether One of Two Random Variables Is Stochastically Larger Than the Other." *Annals of Mathematical Statistics* 18, no. 1: 50–60.

Materechera, S., A. Dexter, and A. M. Alston. 1991. "Penetration of Very Strong Soils by Seedling Roots of Different Plant Species." *Plant and Soil* 135, no. 1: 31–41.

Moss, G. I., K. C. Hall, and M. B. Jackson. 1988. "Ethylene and the Responses of Roots of Maize (*Zea mays* L.) to Physical Impedance." *New Phytologist* 109, no. 3: 303–311.

Pandey, B. K., G. Huang, R. Bhosale, et al. 2021. "Plant Roots Sense Soil Compaction Through Restricted Ethylene Diffusion." *Science* 371, no. 6526: 276–280.

Phalempin, M., N. Jentzsch, J. M. Köhne, et al. 2025. "Soil Structure Development in a Five-Year Chronosequence of Maize Cropping on Two Contrasting Soil Textures." *Soil and Tillage Research* 251: 106561.

Phalempin, M., E. Lippold, D. Vetterlein, and S. Schlüter. 2021a. "An Improved Method for the Segmentation of Roots From X-Ray Computed Tomography 3D Images: Rootine v. 2." *Plant Methods* 17, no. 1: 1–19.

Phalempin, M., E. Lippold, D. Vetterlein, and S. Schlüter. 2021b. "Soil Texture and Structure Heterogeneity Predominantly Governs Bulk Density Gradients Around Roots." *Vadose Zone Journal* 20, no. 5: e20147.

Phalempin, M., U. Rosskopf, S. Schlüter, D. Vetterlein, and S. Peth. 2023. "Can We Use X-Ray CT to Generate 3D Penetration Resistance Data?" *Geoderma* 439: 116700.

Potocka, I., and J. Szymanowska-Pułka. 2018. "Morphological Responses of Plant Roots to Mechanical Stress." *Annals of Botany* 122, no. 5: 711–723.

R Core Team. 2024. *R: A Language and Environment for Statistical Computing*. R Foundation for Statistical Computing. https://www.R-project.org/.

Rivera, M., J. Polanía, J. Ricaurte, G. Borrero, S. Beebe, and I. Rao. 2019. "Soil Compaction Induced Changes in Morpho-Physiological Characteristics of Common Bean." *Journal of Soil Science and Plant Nutrition* 19, no. 1: 217–227.

Schindelin, J., I. Arganda-Carreras, E. Frise, et al. 2012. "Fiji: An Open-Source Platform for Biological-Image Analysis." *Nature Methods* 9, no. 7: 676–682.

Schmidt, S., A. G. Bengough, P. J. Gregory, D. V. Grinev, and W. Otten. 2012. "Estimating Root-Soil Contact From 3d x-Ray Microtomographs." *European Journal of Soil Science* 63, no. 6: 776–786.

Schoonderbeek, D., and J. F. T. Schoute. 1994. "Root and Root-Soil Contact of Winter Wheat in Relation to Soil Macroporosity." *Agriculture, Ecosystems & Environment* 51, no. 1: 89–98.

Stirzaker, R., J. Passioura, and Y. Wilms. 1996. "Soil Structure and Plant Growth: Impact of Bulk Density and Biopores." *Plant and Soil* 185, no. 1: 151–162.

Veen, B. W., M. van Noordwijk, P. de Willigen, F. R. Boone, and M. J. Kooistra. 1992. "Root-Soil Contact of Maize, as Measured by a Thin-Section Technique. Part 3: Effects on Shoot Growth, Nitrate and Water Uptake Efficiency." *Plant and Soil* 139, no. 1: 131–138.

Vetterlein, D., E. Lippold, S. Schreiter, et al. 2021. "Experimental Platforms for the Investigation of Spatiotemporal Patterns in the Rhizosphere—Laboratory and Field Scale." *Journal of Plant Nutrition and Soil Science* 184, no. 1: 35–50.

Vetterlein, D., M. Phalempin, E. Lippold, et al. 2022. "Root Hairs Matter at Field Scale for Maize Shoot Growth and Nutrient Uptake, but Root Trait Plasticity Is Primarily Triggered by Texture and Drought." *Plant and Soil* 478, no. 1: 119–141.

Wankmuller, F. J. P., L. Delval, P. Lehmann, et al. 2024. "Global Influence of Soil Texture on Ecosystem Water Limitation." *Nature* 635, no. 8039: 631–638.

Wendel, A. S., S. L. Bauke, J. C. Ileperuma, K. Funken, K. Frindte, and C. Knief. 2025. "Implications of Reduced Root-Soil Contact for Microbial Rhizosphere Establishment and Early Plant Growth Performance." *Soil Biology and Biochemistry* 207: 109816.

Zhang, J., Z. Liu, E. J. Farrar, et al. 2025. "Ethylene Modulates Cell Wall Mechanics for Root Responses to Compaction." *Nature*: 1–8.

Zhu, M., C.-W. Hsu, L. L. Peralta Ogorek, et al. 2025. "Single-Cell Transcriptomics Reveal How Root Tissues Adapt to Soil Stress." *Nature* 642: 1–9.

Supporting Information

Additional supporting information can be found online in the Supporting Information section. **Data S1:** Supporting Information.